

Novel Technique of Contact Force Vector Determination Aimed at Control of Service Robot Arm and Estimation of Environment Stiffness

Dzmitry Tsetserukou, Naoki Kawakami, and Susumu Tachi

Department of Information Physics and Computing, University of Tokyo, Tokyo, Japan
(Tel : +81-3-5841-6917; E-mail: dima_teterukov@ipc.i.u-tokyo.ac.jp)

Abstract: In this paper, we focus on the approach to calculation of the applied force vector at any point of the robot arm and its technical realization. The experimental results validate the ability of the proposed method to trace the contact point position and to estimate force vector accurately. The technique of calculation of contacting object stiffness during collision is elaborated and experimentally examined. The algorithm of contact transition control considering the environment stiffness value and its application for tactile interaction with surroundings are discussed.

Keywords: Sensitive robot arm, robot-environment interaction, contact transition control.

1. INTRODUCTION

In the past decade, many researches have studied how to avoid unexpected collision of robot with environment or human beings. Several effective collision avoidance strategies were developed. Lumelsky *et al.* [1] proposed to cover manipulator with optical proximity sensors capable of detecting nearby objects. The high-speed vision system attached to the robot arm allows real-time collision avoidance [2]. However, even such complex and skilled sensory system as human beings have cannot avert collisions in our daily lifetime and we must presume such situation during robot operation. Furthermore, such tasks under human supervision as transporting the object, leading the robot tip via force-following, performing the assembling tasks, require the processing algorithm of contact state.

Instead of the general concept of collision avoidance by means of deliberate shunning of contact, we propose the concept of collision avoidance through interaction. The main advantage here is that during contact we can acquire additional information about the object, namely, its stiffness, texture, shape, and relative position.

Conventional approaches to controlling the physical interaction between a manipulator and environment are based on impedance control of a robot arm according to applied force vector measured at the manipulator wrist [3]. However, the rest parts of the robot body (forearm, elbow, upper arm, shoulder, and torso) are presenting significant danger not only for human being, but also for the robot structure itself.

Distributed optical joint torque sensors and local admittance controllers endow our robot arm with the distinctive capability of safe interaction with surroundings along entire manipulator surface. The developed robot arm is shown in Fig. 1(a). The coordinate systems fixed to the joints and connected to the arbitrary contact points are given in Fig. 1(b).

The paper focuses on approach to determination of the applied force vector at each point of the robot arm. This information is essential to plan collision avoidance trajectory, structure the environment, and communicate with humans intelligently. The proposed method takes

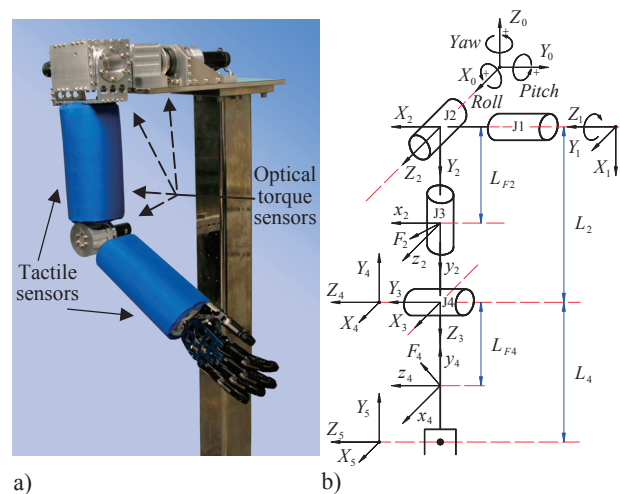


Fig. 1 Robot arm and frame assignments.

advantages of the tactile sensor, enabling to detect coordinates of the contact point, and the distributed joint torque sensors to measure exerted torques and force vector direction on the entire robot arm surface (including joints). This method originates from human tactile system. Very fine special resolution of the human skin allows performing tactile discrimination of surface texture by fingertips. However, it has moderate ability to estimate the exerted force, the job that muscles do. They generate torque at the skeletal joints balancing such external forces as gravity, mechanical constraints of joints, inertial forces, and contact forces. Each muscle produces a torque at a joint that is the product of its contractile force and its moment arm at that joint [4]. Hence, by estimation of the tension of the corresponding muscles, we can define the acting force as well as the force direction.

In the paper we also address contact transition control which enables estimation of contacting object stiffness and trajectory following targeted by object surface.

The remainder of the paper is structured as follows. Section 2 introduces the approach to calculation of contact force vector. The robot sensory system and experimental results of measurement of contact force vector are presented in Section 3. The methods for

contact state recognition and estimation of contacting object stiffness are detailed in Section 4. In Section 5, we conclude the paper and discuss the future work.

2. CALCULATION OF CONTACT FORCE VECTOR

The proposed algorithm of computing the force vector at any contact point on entire teleoperated robot arm employs information about the contact point coordinates and joint torque values.

The forces ${}^i f_i$ acting in the coordinate system of each joint produce moments ${}^i n_i$ (Eq. (1)). The joint torques are derived by taking Z component of the moments applied to the link (Eq. (3)).

$${}^i n_i = {}^{i+1}R^{i+1} n_{i+1} + {}^i P_{C_i} \times {}^i F_i + {}^i P_{i+1} \times {}^{i+1}R^{i+1} f_{i+1} \quad (1)$$

$${}^i f_i = {}^{i+1}R^{i+1} f_{i+1} + {}^i F_i \quad (2)$$

$$\tau_i = {}^i n_i^T \hat{Z}_i, \quad (3)$$

where ${}^{i+1}R$ is the matrix of rotation between links $i+1$ and i calculated using Denavit-Hartenberg notation; ${}^i P_{i+1}$, ${}^i P_{C_i}$ are the vectors locating the origin of the coordinate system $i+1$ in the system i , and contact point, respectively; ${}^i F_i$ is the contact force.

Let us consider the case when force is applied to the upper arm of the robot. Using the Eq. (1), (2) we have:

$${}^2 n_2 = \begin{bmatrix} 0 \\ L_{F2} \\ 0 \end{bmatrix} \times \begin{bmatrix} F_{2x} \\ F_{2y} \\ F_{2z} \end{bmatrix} = \begin{bmatrix} L_{F2} F_{2z} \\ 0 \\ -L_{F2} F_{2x} \end{bmatrix};$$

$${}^1 n_1 = \begin{bmatrix} s_2 & c_2 & 0 \\ 0 & 0 & 1 \\ c_2 & -s_2 & 0 \end{bmatrix} \begin{bmatrix} L_{F2} F_{2z} \\ 0 \\ -L_{F2} F_{2x} \end{bmatrix} = \begin{bmatrix} L_{F2} F_{2z} s_2 \\ -L_{F2} F_{2x} \\ L_{F2} F_{2z} c_2 \end{bmatrix}. \quad (4)$$

The components of the applied force vector and force magnitude are derived from:

$$F_{2x} = \tau_2 / (-L_{F2}); \quad F_{2z} = \tau_1 / (L_{F2} c_2);$$

$$F_2 = \sqrt{(F_{2x})^2 + (F_{2z})^2}. \quad (5)$$

The value of the applied force projection on the axis Y is not required because the upper arm cannot move in this direction. For the case when the force acts on the forearm we have the following algorithm to obtain the contact force vector:

$$F_{4y} = \frac{(\tau_2 + F_{4z}(L_{F4} c_3 c_4 + L_2 c_3) + F_{4x}(L_{F4} s_3 + L_2 s_3 c_4))}{(L_2 s_3 s_4)}$$

$$F_{4x} = \tau_4 / L_{F4}; \quad F_{4z} = \tau_3 / (L_{F4} s_4), \quad (6)$$

where c_2 , c_3 , c_4 , s_3 , and s_4 are abbreviations for $\cos(\theta_2)$, $\cos(\theta_3)$, $\cos(\theta_4)$, $\sin(\theta_3)$, and $\sin(\theta_4)$, respectively; L_2 , L_{F2} , and L_{F4} are the lengths of the moment arms.

3. ROBOT SENSORY SYSTEM AND EXPERIMENTAL RESULTS

3.1 Sensory system

For practical implementation of the proposed approach we developed sensory system of the robot arm which includes tactile skin and optical torque sensors distributed into each joint.

The robot arm is covered with Kinotex tactile sensor measuring the pressure intensity through amount of backscattered light by photodetector [5]. The sensitivity, resolution, and dynamic range of this artificial skin are comparable to those of a human. The taxels displaced with 21.5 mm in X and 22 mm in Y direction make up 6x10 array. The developed program code analyses the tactile pattern and calculates the number of contacts and the center of gravity of the contact pattern based on the pressure distribution information.

In technical specifications of the Kinotex sensor, the ability of force measurement is indicated. However, the following shortcomings complicate the accurate measurement of the applied force: temperature dependency of the transducer constant, fragility while mechanical overloading, large hysteresivity, high non-linearity of the output, limited sensing range, etc. Additionally, the tactile sensors detect and measure the spatial distribution of forces perpendicular to a predetermined sensory area and, hence, cannot evaluate the vector of applied force. Thus, the most appropriate application of such tactile sensors is the contact area recognition and the measurement of relative pressure distribution in the contact region on the robot body surface. The task of load measurement is accomplished by the developed optical torque sensors enabling torque measurement with high accuracy.

In order to recognize the contact region, we employed the watershed algorithm, an image processing segmentation technique that splits an image into areas based on the topology of the image [6]. The intuitive idea underlying the approach comes from the field of topography: a drop of water falling on the relief follows a descending path and ultimately reaches a minimum. The adopted algorithm is processed as follows: departing from the local maximum, the new taxel is included into the contact area only if within the 3x3 array surrounding it there is an other taxel of greater or equal pressure intensity already included into the water stream.

The accurate estimation of the contact point can be obtained by computing the center of gravity of the contact pattern $c(x_c, y_c)$ of the neighborhood Ω by:

$$c(x_c, y_c) = \left(\frac{\sum_{x_i, y_i \in \Omega} x_i f_i(x_i, y_i)}{\sum_{x_i, y_i \in \Omega} f_i(x_i, y_i)}, \frac{\sum_{x_i, y_i \in \Omega} y_i f_i(x_i, y_i)}{\sum_{x_i, y_i \in \Omega} f_i(x_i, y_i)} \right), \quad (7)$$

where $f_i(x_i, y_i)$ is the pressure intensity level of the taxel i with coordinates (x_i, y_i) .

The example of contact area image by using Kinotex skin is presented in Fig. 2.

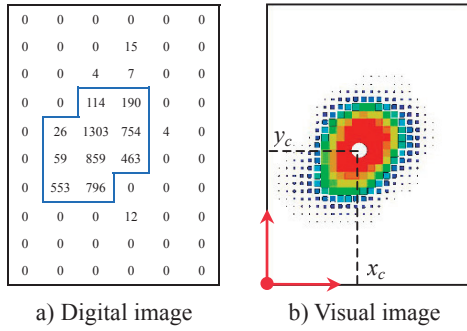


Fig. 2 Representations of the contact area.

In order to facilitate the realization of torque measurement in each arm joint, we developed new optical torque sensors based on results presented in [7]. The novelty of our method is application of the ultra-small size photointerrupter (PI) RPI-121 as sensitive element to measure relative motion of sensor components. The dimensions of the PI (3.6 mm × 2.6 mm × 3.3 mm) and its weight of 0.05 g allow realization of compact design. The optical torque sensor is set between the driving shaft of the harmonic transmission and driven shaft of the joint (Fig. 3). When the load is applied to the robot joint, the magnitude of the output signal from the PI corresponds to the exerted load.

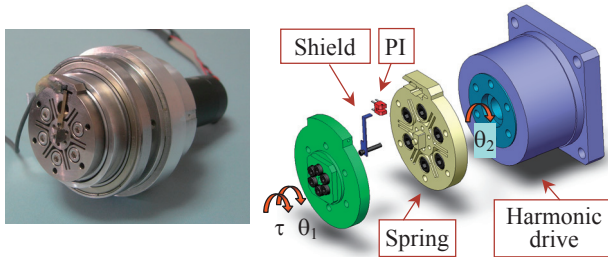


Fig. 3 Torque sensor of the elbow joint.

The spring members attached to the first, second, and third/fourth joints were designed to measure torque of ± 12.5 Nm, ± 10.5 Nm, ± 4.5 Nm, and have resolution of 10.77 mNm, 9.02 mNm, 4.31 mNm, respectively. Each sensor was calibrated by means of attachment of reference weights to the lever arm. Non-linearity of 2.5 % of Full Scale was calculated using maximum deviated value from the best-fit line.

The developed optical torque sensors have high dependability, good accuracy (even in electrically noisy environment), low price, compact sizes, light weight, and easy manufacturing procedure.

3.2 Experimental results

To evaluate the feasibility of the proposed approach, the experiments were conducted for calculation of the contact force vector acting on the upper arm.

During the experiment the object was moved along the upper arm surface according to the curve shown in

Fig. 4(c). While contacting, the torque values measured at the first and second joint (τ_1 , τ_2) vary in accordance with Fig. 4(a). The contact force vector projections (F_{2x} , F_{2y}) and force vector length F_2 obtained from Eq. (5) are represented in Fig. 4(b). The trajectory of the end point of the contact force vector is shown in Fig. 4(d).

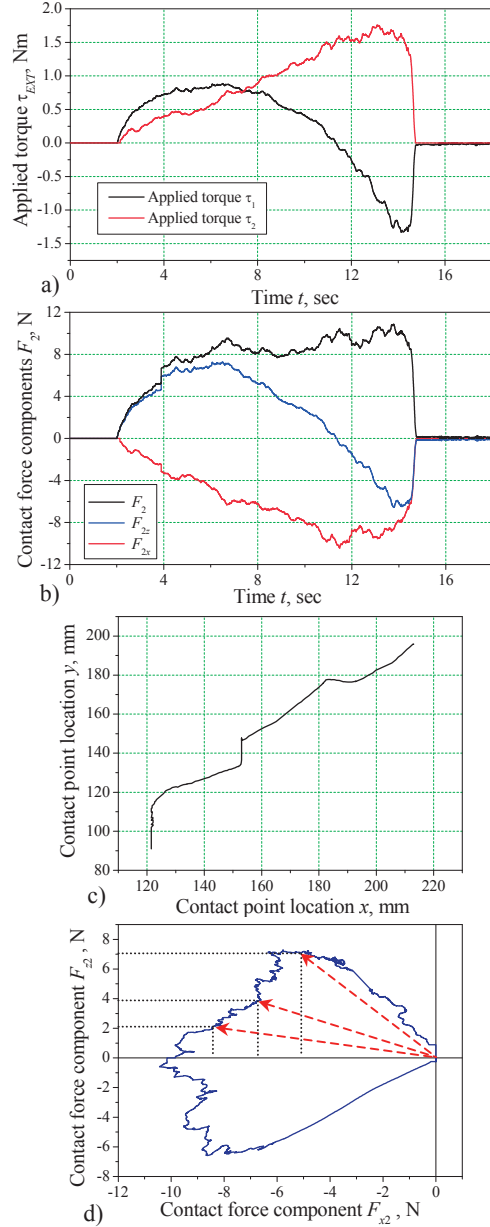


Fig. 4 Experimental results.

Robot sensory system and proposed algorithm have demonstrated ability of contact force vector calculation.

4. ROBOT-ENVIRONMENT INTERACTION

4.1 Contact state recognition

During the first stage of control the robot links rotate until one of them contacts the object. First, the algorithm of contact detection must be elaborated.

In addition to contact force, torque sensors continuously measure the gravity and inertial load. As

robot arm moves with low angular speed, the inertial load component can be disregarded. Let us consider gravity torque calculation in the case when robot arm performs only planar motion, and only the first and fourth joints operate (Fig. 5).

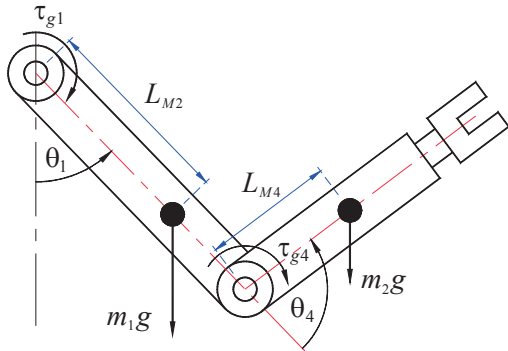


Fig. 5 Robot arm subjected to gravity loading.

The Newton-Euler dynamics formulation was adopted to calculate reference value of the gravity torques. The gravity torques acting in the first τ_{g1} and fourth joints τ_{g4} are derived from:

$$\begin{aligned} \tau_{g1} &= m_2 g (L_{M4} \sin(\theta_1 + \theta_4) + L_2 \sin(\theta_1)) + m_1 g L_{M2} \sin(\theta_1) \\ \tau_{g4} &= m_2 g L_{M4} \sin(\theta_1 + \theta_4), \end{aligned} \quad (8)$$

where m_1 and m_2 are the point masses of the first and second link, respectively; L_{M2} and L_{M4} are the distances from the first and second link origins to the centers of mass, respectively.

The experiment with the fourth joint of the robot arm was conducted in order to measure the gravity torque (Fig. 6(a)) and to estimate the error by comparison with reference model (Fig. 6(b)).

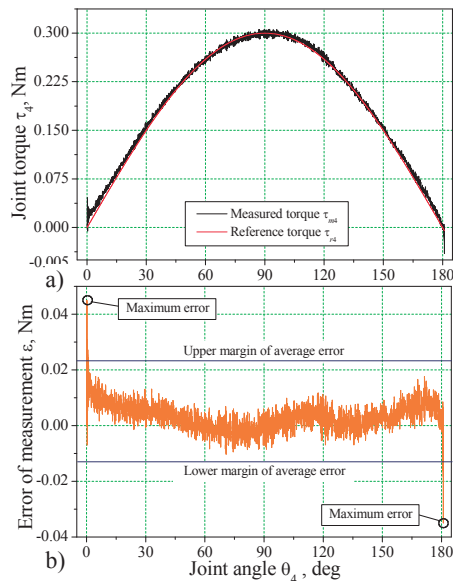


Fig. 6 Experimental results of gravity measurement.

As can be seen from Fig. 6, the pick values of the gravity torque estimation error arise at the start and stop stages of the joint rotation. The reason of this is high

inertial loading that provokes the vibrations during acceleration and deceleration transient. This disturbance can be evaluated by using accelerometers and excluded from further consideration. Observing the measurement error plot, we can assign the relevant threshold that triggers control of constraint motion.

4.2 Estimation of contacting object stiffness

During contact transition we can acquire information about collision danger of contacting object through its stiffness estimation. This can be done by establishing stiff contact through PD control of robot arm with high P-gain and setting the high threshold value. For the following experimental results the threshold was chosen as high as 0.05 Nm. The robot was commanded to follow the trajectory in free space with constant angular velocity. An object was placed on this path so that the second link will contact the object. The joint torque was recorded for the fourth joint while contacting with object. The Figs. 7(a)~7(e) show experimental results when link comes into contact with objects having different stiffness varying from very low rate to very high, namely, piece of sponge, rubber sponge, rubber, chemical wood, and aluminum, respectively. The time derivative of torque during impact is given in Fig. 7(f).

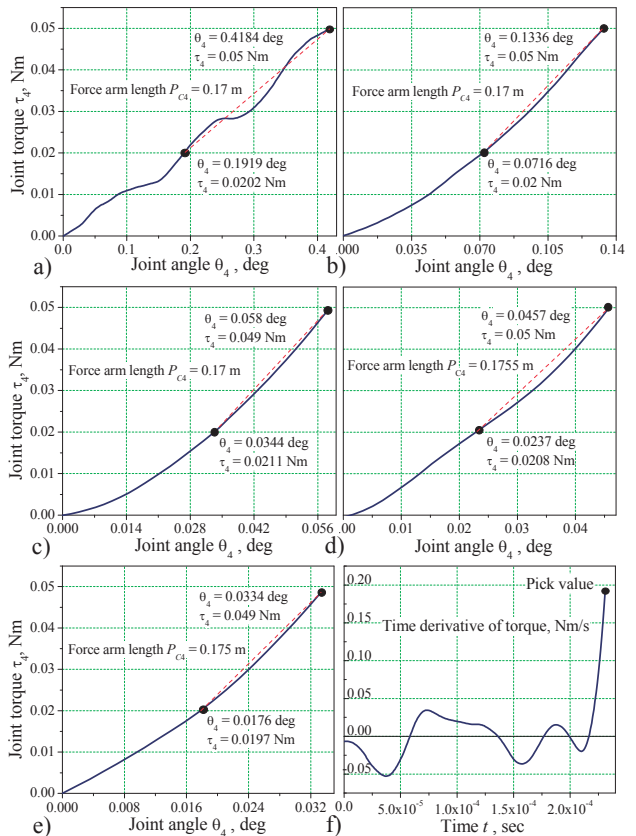


Fig. 7 Experimental results of stiffness estimation.

It is apparent from the above presented plots that the stiffer object comes into contact with robot arm the smaller angle the joint rotates. Heterogeneous nature of sponge material explains highly non-linear behavior of stiffness curve (Fig. 7(a)).

The elastic deformation of the object and inherent compliance of the robot joints lead to rotation of robot arm of angle $\Delta\theta_i$ during contact transience (Fig. 8).

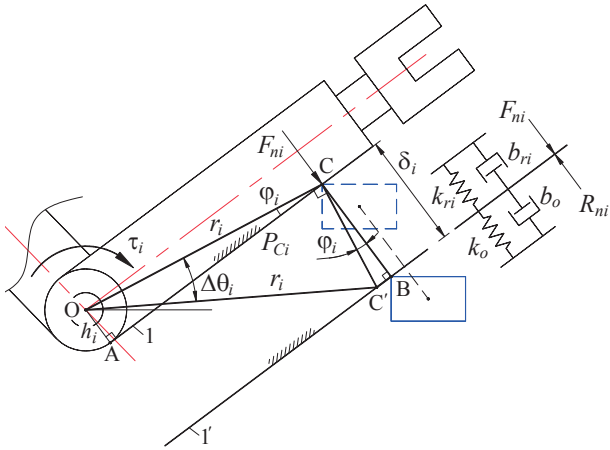


Fig. 8 The scheme for elastic deformation calculation.

The distance, which contact point C on the robot link surface 1 moves perpendicularly to the radius r_i under torque $\Delta\tau_i$, is equal to $r_i\Delta\theta_i$ (since the angle $\Delta\theta_i$ is fairly small). The unknown angle φ_i can be found by noting that $\angle CCB = \angle OCA = \varphi_i$:

$$\varphi_i = \arctan\left(\frac{OA}{CA}\right) = \arctan\left(\frac{h_i}{P_{C_i}}\right), \quad (9)$$

where h_i equals half of the robot link thickness (for forearm $h = 0.03$ m).

From the right triangle $\Delta CBC'$ the total elastic deformation is calculated as:

$$\delta_i = \Delta\theta_i r_i \cos(\varphi_i). \quad (10)$$

Radius of contact point trajectory r_i is found through consideration of right triangle ΔCAO as $r_i = \sqrt{P_{C_i}^2 + h_i^2}$.

Now, we can easily solve for total stiffness:

$$k_i = \frac{F_{ni}}{\delta_i} = \frac{\Delta\tau_i}{P_{C_i} \Delta\theta_i r_i \cos(\varphi_i)} = \frac{\Delta\tau_i}{P_{C_i} \Delta\theta_i \sqrt{P_{C_i}^2 + h_i^2} \cos(\arctan(h_i/P_{C_i}))}. \quad (11)$$

By linear approximation, we take into account only two values of θ_i for τ_i nearest to 0.02 Nm and 0.05 Nm. Then, from the experimental diagrams (Figs. 7(a)~7(e)) we obtain $\Delta\theta_i$ and $\Delta\tau_i$ listed in Table 1.

Table 1 Findings from experimental diagrams.

Parameter	Sponge	Rubber sponge	Rubber	Wood
$\Delta\theta_i \cdot 10^{-4}$ [rad]	39.53	10.82	4.12	3.84
$\Delta\tau_i \cdot 10^{-2}$ [Nm]	2.98	3.0	2.79	2.92

The total elastic deformation δ_i is made up of elastic deformation caused by object compliance δ_o and one generated by joint flexibility δ_{r_i} . That is, we can write:

$$\delta_i = \frac{F_{ni}}{k_i} = \delta_o + \delta_{r_i} = \frac{R_{ni}}{k_o} + \frac{F_{ni}}{k_{r_i}}, \quad (12)$$

where R_{ni} is the reaction, absolute value of which equals F_{ni} ; k_o and k_{r_i} are stiffness of the object and stiffness of robot link, respectively.

The coefficient k_{r_i} is mainly defined by torque sensor stiffness, harmonic drive stiffness, structural flexibility, and P-gain magnitude. Detailed examination has showed that complex theoretical model of robot link stiffness can hardly provide accurate estimation of k_{r_i} . Rather, we can set the value of robot link stiffness close to total stiffness in the most hard contact case. This assumption is valid because during impact with hard environment, such as aluminum plate, the contact deformation of the object is too small to be accounted ($k_o \approx \infty$). Thus, from the data listed in Fig. 7(e) and using Eqs. (9) ~ (11) we derive unknown value of k_{r_i} :

$$k_{r_i} = \frac{0.0293 \text{ Nm}}{0.175 \cdot 2.758 \cdot 10^{-4} \cdot 0.1776 \cdot 0.986 \text{ m}^2} = 3468.6 \frac{\text{N}}{\text{m}}$$

The stiffness of the objects made from sponge, rubber sponge, rubber, and chemical wood are calculated from the following equation:

$$k_o = \frac{k_{r_i} \cdot k_i}{k_{r_i} - k_i}, \quad (13)$$

where k_i is defined by Eq. (11). Derived values of k_i and k_o are given in Table 2.

Table 2 Total stiffness and object stiffness.

Parameter	Sponge	Rubber sponge	Rubber	Wood
k_i [N/m]	260.84	959.3	2343.78	2469.04
k_o [N/m]	282.04	1325.92	7223.94	8562.90

The obtained results demonstrate strong correspondence of correlation among calculated object stiffness with that of real objects. Naturally, the actual stiffness of colliding environment differs from calculated one with finite error. To achieve high accuracy, specific equipment is needed. However, our aim was only assessment of the danger level of robot arm collision with object. Specifically, we can define that sponge and rubber sponge material are safe for interaction but rubber, wood, and metal pose threat while striking the robot arm. Consequently, we have succeeded in solving main task, that is, object classification by getting information about stiffness during impact.

In case when collision must be robustly detected without consideration of object property, the value of

time derivative of torque can be used to judge the impact value (Fig. 7(f)).

4.3 Control of physical interaction of robot arm with surroundings

As soon as the joint torque value exceeds the threshold, the control is transmitted to local admittance controller. Thus, on the last stage of contact transience compliant interaction is provided with predetermined dynamics. The desired impedance properties of i -th joint of manipulator can be expressed as:

$$J_{di} \Delta \ddot{\theta}_i + D_{di} \Delta \dot{\theta}_i + K_{di} \Delta \theta_i = \tau_{EXTi}; \Delta \theta_i = \theta_{ci} - \theta_{di}, \quad (14)$$

where J_{di} , D_{di} , K_{di} are the desired inertia, damping, and stiffness of i -th joint, respectively; τ_{EXTi} is torque applied to i -th joint and caused by external and gravity forces, $\Delta \theta_i$ is the difference between the current position θ_{ci} and desired one θ_{di} .

The remarkable opportunity is that we can establish different dynamic parameters of robot arm interaction with environment according to its stiffness. This is inherent capability of humans, when we collide with stiff objects we tend to soften our muscles as we can.

Another possible application of proposed approach is to structure the environment. At present time, vision system of robots cannot correctly determine the distance to the object in 3D space. Thus, such simple task as taking a cup from table by hand is extremely difficult for robots. By contact interaction, we can define reference coordinate system and reachable working area. As example of such control implementation, the table surface following trajectory and force vector direction at each motion step are shown in Fig. 9.

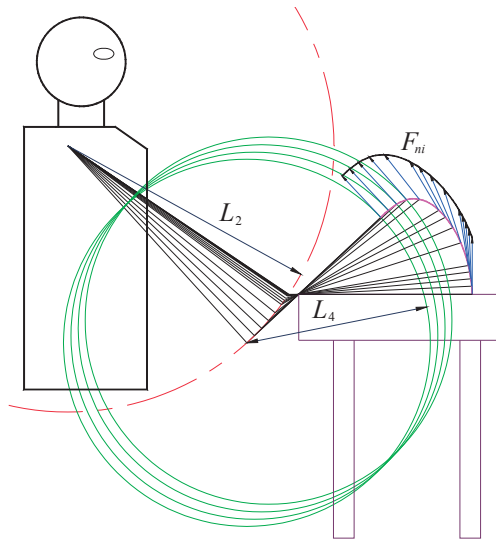


Fig. 9 The table surface following trajectory.

The robot control through tactile interaction would endow the robot with human-like ability to safely interact with environment.

5. CONCLUSIONS AND FUTURE WORK

It was shown experimentally that the developed algorithm and implemented sensory system of the robot arm allow measuring the force direction at any point of the robot arm accurately and robustly.

The main stages of contact transition control were described. Then, we detailed the procedure of contact state recognition. As soon as contact with object is established, the robot arm changes own dynamic parameters according to estimated object stiffness. The presented method of object deformation calculation allowed estimating the level of collision dangerousness. Analysis of experimental results elicited a fact of strong correspondence of correlation among calculated object stiffness with that of real objects.

In the future research we are going to employ the information on force vector and contact point to plan the compliant collision avoidance trajectory autonomously and provide tactile feedback to the operator. We consider that presenting the information about direction and intensity of the contact force vector can greatly improve the collision avoidance strategy realized by operator, in comparison with the conventional contact area tactile feedback. On the next stage we will also realize presented in the paper idea of trajectory following targeted by object surface.

Acknowledgments. The research is supported in part by a Japan Society for the Promotion of Science (JSPS) Postdoctoral Fellowship for Foreign Scholars.

REFERENCES

- [1] V. J. Lumelsky and E. Cheung, "Real-time Collision Avoidance in Teleoperated Whole-sensitive Robot Arm Manipulators", *IEEE Trans. on Systems, Man, and Cybernetics*, Vol. 23, No. 1, pp. 194-203, 1993.
- [2] S. Morikawa, T. Senoo, A. Namiki, M. Ishikawa, "Real-time Collision Avoidance Using a Robot Manipulator with Light-weight Small High-speed Vision System" *IEEE Int. Conf. Robotics and Automation*, Roma, pp. 794-799, 2007.
- [3] F. Caccavael, C. Natale, B. Siciliano, L. Villani, "Six-DOF Impedance Control Based on Angle/Axis Representation", *IEEE Transaction on Robotics and Automation*, Vol. 15, No. 2, pp. 289-300, 1999.
- [4] E. R. Kandel, J. H. Schwartz, T. M. Jessell, *Principles of Neural Science*, McGraw-Hill, New York, 2000.
- [5] Optic Fiber Tactile Sensor Kinotex, Nitta Corporation, "<http://www.nitta.co.jp/>"
- [6] J. Serra, *Image Analysis and Mathematical Morphology*, Academic Press, London, 1982.
- [7] D. Tsetserukou, R. Tadakuma, H. Kajimoto, S. Tachi, "Optical Torque Sensors for Implementation of Local Impedance Control of the Arm of Humanoid Robot", *IEEE Int. Conf. on Robotics and Automation*, Orlando, pp. 1674-1679, 2006.